



2nd International Summer School on Nuclear Glass Wasteform: Structure, Properties and Long-Term Behavior, SumGLASS 2013

## Conversion of nuclear waste into nuclear waste glass: Experimental investigation and mathematical modeling

Pavel Hrma\*

*Pacific Northwest National Laboratory, P.O. Box 999, Richland, Washington, 99352, USA*

---

### Abstract

The melter feed, slurry, or calcine charged on the top of a pool of molten glass forms a floating layer of reacting material called the cold cap. Between the cold-cap top, which is covered with boiling slurry, and its bottom, where bubbles separate it from molten glass, the temperature changes by up to 1000 K. The processes that occur over this temperature interval within the cold cap include liberation of gases, conduction and consumption of heat, dissolution of quartz particles, formation and dissolution of intermediate crystalline phases, and generation of foam and gas cavities. These processes have been investigated using thermal analyses, optical and electronic microscopies, x-ray diffraction, as well as other techniques. Properties of the reacting feed, such as heat conductivity and density, were measured as functions of temperature. Investigating the structure of quenched cold caps produced in a laboratory-scale melter complemented the crucible studies. The cold cap consists of two main layers. The top layer contains solid particles dissolving in the glass-forming melt and open pores through which gases are escaping. The bottom layer contains bubbly melt or foam where bubbles coalesce into larger cavities that move sideways and release the gas to the atmosphere. The feed-to-glass conversion became sufficiently understood for representing the cold-cap processes via mathematical models. These models, which comprise heat transfer, mass transfer, and reaction kinetics models, have been developed with the final goal to relate feed parameters to the rate of glass melting.

© 2014 The Authors. Published by Elsevier Ltd.

Selection and peer-review under responsibility of the scientific committee of SumGLASS 2013.

*Keywords:* Type your keywords here, separated by semicolons ;

---

---

\* Corresponding author. Tel.: 509-372-4581.

*E-mail address:* Pavel.Hrma@pnl.gov

## 1. Introduction

A melter feed is composed of nuclear waste mixed with glass-forming and glass-modifying additives, whether in the form of chemicals, minerals, or frit. The conversion of the melter feed proceeds almost entirely within the cold cap, a layer of the reacting feed floating on the pool of molten glass in the Joule-heated or induction-heated melter. Heat from the glass pool is transferred to the cold cap by convection that can be enhanced through gas bubbling (Matlach et al., 2013). Inside the cold cap, the heat is transferred via conduction. The rate of the feed-to-glass conversion (i.e., the rate of melting) is controlled by the heat delivered to the cold cap from the bottom and top surfaces, but the chemical and physical form of the feed affects the rate at which the incoming heat is received (Hrna et al., 2010; Schweiger et al., 2010).

In this contribution, we consider a cold cap in a Joule-heated melter in which feed is charged as a slurry of waste blended with glass additives in the form of chemicals and minerals. Such a cold cap consists of two distinct portions as shown in Fig. 1 (Pokorny and Hrna, 2012 and 2014). Major gas-evolving reactions occur in the upper portion where the open pores allow the reaction gases to escape. In the lower portion, the continuous glass-forming melt contains dissolving and precipitating solids and gas bubbles from residual feed reactions (primary foam) and from redox reactions within the melt (secondary foam). The foam layers hinder heat flow to the cold cap. As illustrated in Fig. 1, and experimentally demonstrated by Dixon et al., (2013), bubbles in both primary and secondary foam coalesce and merge into larger cavities that eventually burst into the plenum space above the cold cap. In Fig. 1,  $Q$  indicates the heat flux and  $T$  the temperature; subscript  $U$  denotes the upper space,  $T$  the top surface,  $B$  the bottom,  $P$  primary foam,  $C$  cavity, and  $S$  secondary foam. Primary foam can be avoided or at least minimized by releasing most, if not all, batch gases before the glass-forming melt becomes connected while delaying the development of a continuous glass-forming melt until reaction gases are fully released.

This paper presents a mathematical model of the cold cap and selected results based on the properties of a high-alumina, high-level waste. Selected experimental results for cold caps generated in a laboratory-scale melter also are shown.

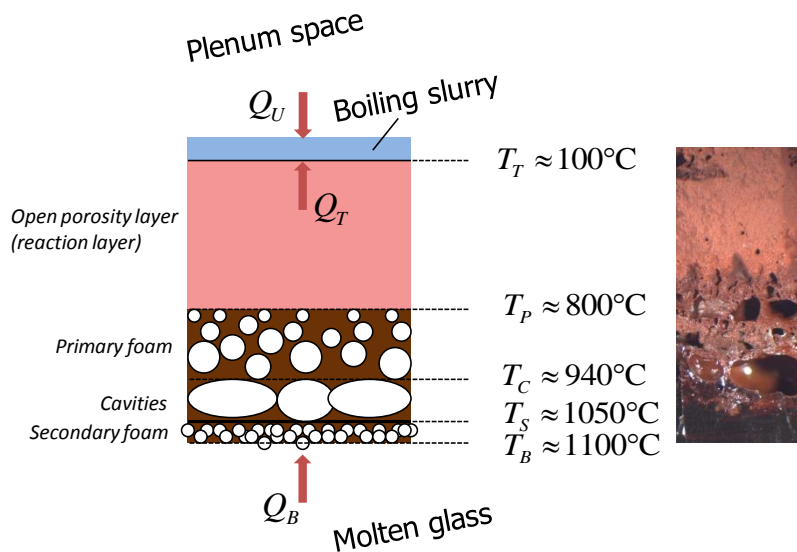


Fig. 1. Schematic illustration of a cold cap, and a section through a cold cap produced in a laboratory-scale melter (Pokorny and Hrna, 2012 and 2014; Dixon et al., 2013).

## 2. Cold cap model

The cold-cap mathematical model describes the transfer of mass and heat through the layer of reacting material. A simple one-dimensional form of the energy balance can be expressed as Eq. (1) (Pokorný and Hрма, 2014; Hрма, 1982; Schill, 1982; Schill et al. 2007; Hрма et al., 2012)

$$\rho_b c_p^{Eff} \frac{dT}{dt} = (j_b c_p^{Eff} + j_g c_g) \frac{dT}{dy} - \lambda \frac{d^2 T}{dy^2} \quad (1)$$

where  $\rho$  is the density,  $T$  is the temperature,  $y$  is the vertical coordinate,  $c_p$  is the heat capacity,  $\lambda$  is the heat conductivity, and  $j$  is the mass flux; subscripts  $b$  and  $g$  denote the condensed phase and the gas phase, respectively, and superscript  $Eff$  indicates the effective value. The condensed-phase mass flux is  $j_b = \alpha_b j_T$ , where  $\alpha_b$  is the mass fraction of condensed phase, and  $j_T$  is the mass flux of dry feed entering the cold cap. The gas-phase mass flux is expressed as  $j_g = (\alpha_b - \alpha_M) j_T$ , where  $\alpha_M$  is the mass fraction of the condensed phase at the cold-cap bottom.

Solving Eq. (1) for appropriate boundary conditions (the temperatures at the top and bottom of the cold cap, the foaminess, and the fraction of heat coming from above) is possible if the key properties of the reacting feed ( $\rho_b$ ,  $c_p^{Eff}$ ,  $c_g$ ,  $\lambda$ , and  $\alpha_b$ ) are known as functions of temperature and heating rate. As described below, these functions were experimentally determined for a melter feed formulated for a high-alumina, high-level waste.

The melter feed bulk density,  $\rho_b$ , was obtained from pellet expansion data (Fig. 2) (Henager et al., 2011). The volumes of both loose dry feed and dry feed pellets changed little in response to heating initially while gases were evolving and escaping through open pores. Starting at  $\sim 700^\circ\text{C}$ , the feed began to shrink to a minimum volume at the primary foam temperature (Fig. 1),  $T_p$ , above which the glass-forming melt became connected and open pores turned into bubbles trapping residual gases. As temperature increased above  $T_p$ , the melt expanded to foam that peaked at the cavity collapsing temperature,  $T_c$ , above which foam rapidly collapsed to a bubble-free melt.

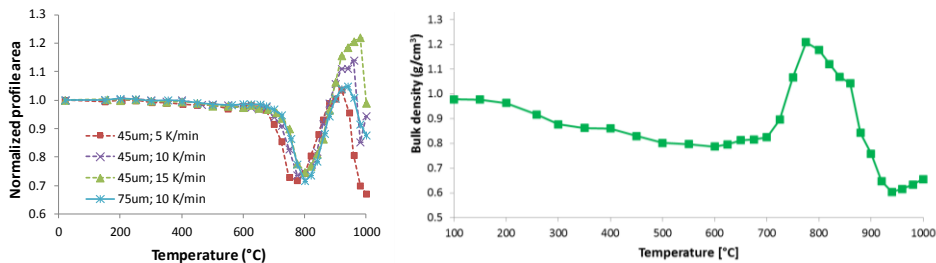


Fig. 2. Normalized melter-feed-pellet profile area versus temperature and heating rate (left). Effect of temperature on the density of a feed sample heated at 5 K/min (right).

The degrees of conversion related to mass change,  $\alpha_b(T)$  and  $\alpha_M$ , were determined by the thermogravimetric analysis (Pokorný et al., 2012; Pierce et al., 2012a and 2012b). The differential scanning calorimetry was employed (Chun et al., 2013) to determine the effective heat capacity of the condensed phase,  $c_p^{Eff} = c_p + \Delta H d\alpha_H/dT$ , where  $c_p$  is the true heat capacity,  $\Delta H$  is the total reaction heat ( $\text{J kg}^{-1}$ ), and  $\alpha_H$  is the degree of conversion related to reaction heat. The heat capacity of carbon dioxide was used to approximate  $c_g$ .

The heat conductivity was obtained from the temperature field measured by an array of thermocouples positioned in the feed placed in a tall cylindrical crucible heated from the sides (Pokorný et al., 2013b). The value of  $\lambda$  was determined as a function of temperature by fitting the Eq. 2 to data:

$$\rho_b c_p^{Eff} \frac{dT}{dt} = \frac{1}{r} \frac{\partial}{\partial r} \left( r \lambda \frac{\partial T}{\partial r} \right) \quad (2)$$

where  $r$  is the radial coordinate. As seen in Fig. 3, the value of  $\lambda$  was almost constant below 700°C and then rapidly increased within the temperature interval from 700°C to  $T_P$  (the temperature at which glass-forming melt consolidates into a continuous phase). As the feed was turning into primary foam within the temperature interval from  $T_P$  to  $T_C$ , the value of  $\lambda$  dropped to a minimum and then increased, probably because of radiative heat transfer through growing bubbles. When the bubbles were gone, the value of  $\lambda$  approached the conductivity of the bubble-free melt ( $\sim 1.4 \text{ W m}^{-1} \text{ K}^{-1}$ ).

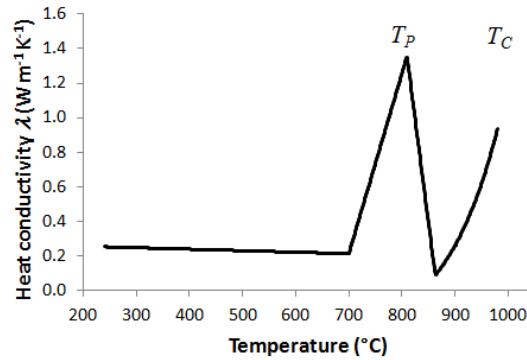


Fig. 3. Heat conductivity of reacting feed versus temperature.

Fig. 4 displays the main results of mathematical simulation of the cold cap (Pokorny and Hrma, 2014). Because the  $\lambda(T)$  function shown in Fig. 3 was only partially available at the time of model computation, a somewhat different  $\lambda(T)$  function was used in the model, but this should not affect the trends observed. The diagrams in Fig. 4 show that the melting rate increases and cold-cap thickness decreases as the temperature at the bottom of the cold cap increases and the melt foaminess decreases. The foaminess of a liquid is defined as the time the incoming gas (from below) takes to pass through the foam layer. Thus, it is a measure of the propensity of a melt to create secondary foam. The secondary foam layer thickness is thus strongly affected by melt foaminess, but also by the cold cap bottom temperature via the flux of gases from the melt below the cold cap (Hrma, 1990).

The melting rate also is affected by the fraction of heat supplied to the cold cap from the head (plenum) space ( $f_{\text{plenum}}$ ) and, of course, by the chemical nature of melter feed components, such as the alumina source. The melting rate of the feed with boehmite ( $\text{AlO}(\text{OH})$ ) is higher than the melting rate of the feed with gibbsite ( $\text{Al}(\text{OH})_3$ ) because boehmite has a considerably lower conversion heat.

Apart from these basic relationships, the model can estimate various other features of the cold-cap structure, such as distributions of temperature, bulk and gas-phase velocities, and local heating rate within the cold cap (Pokorny and Hrma, 2014). These distribution functions are sensitive to the local values of open porosity, heat conductivity, gas-evolution rate, melt connectivity, foam density, etc. Moreover, the model can simulate quartz dissolution within the cold cap, including the size of the quartz particles leaving the cold cap, the formation and dissolution of intermediate crystalline phases, such as hematite and spinel, including the fraction and size of spinel crystals entering the melt convection currents (spinel settling may affect melter performance, see Mika et al., 2000; Hrma and Vienna, 2000; Matyas et al., 2010). These additional features require knowledge of kinetic equations that relate various feed reactions to the temperature and the rate of heating (Dolan and Misture, 2004; Hrma et al., 2011; Hrma and Marcial, 2011; Pokorny et al., 2013a).

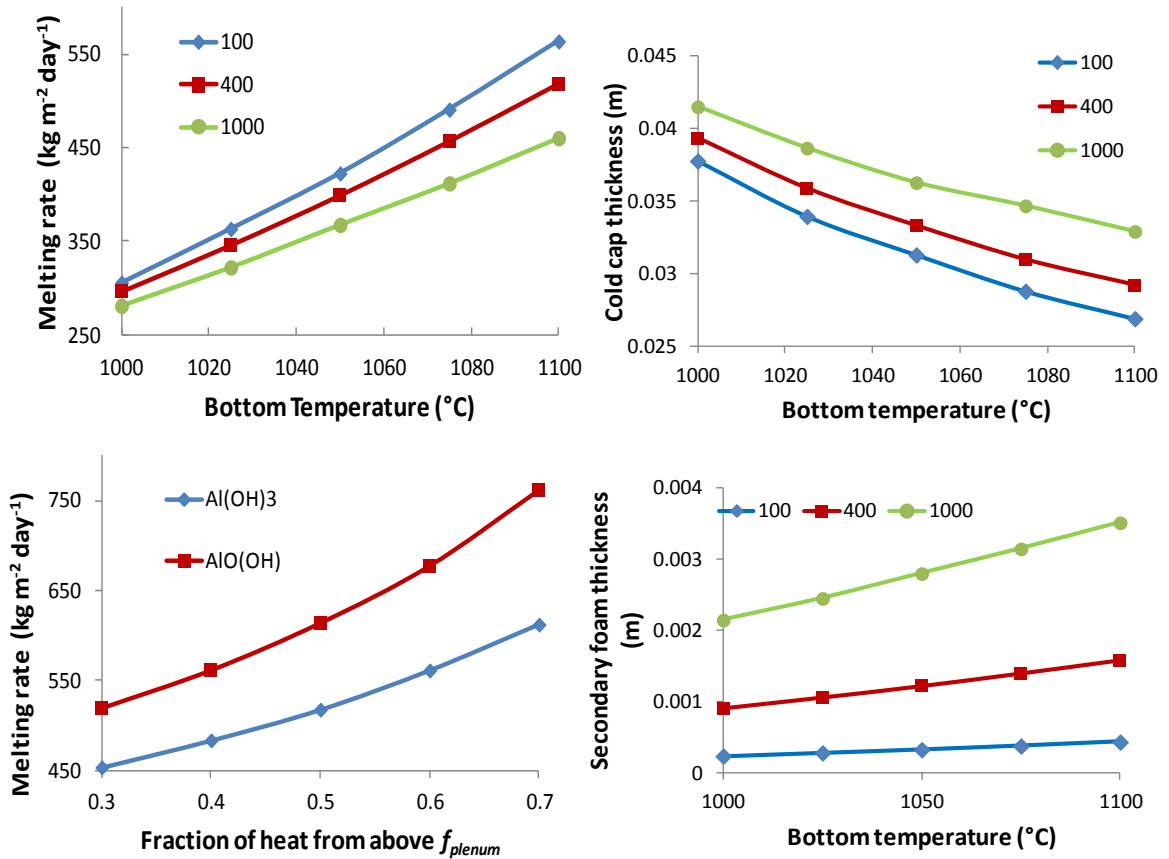


Fig. 4. Melting rate (top left) and cold-cap thickness (top right) versus cold cap bottom temperature and melt foaminess (s); melting rate versus fraction of heat flow from above for feeds with different alumina sources (bottom left); secondary foam layer thickness versus cold cap bottom temperature and melt foaminess (bottom right).

### 3. Laboratory-scale melter

Cold caps from glass melters are difficult to access, and representative samples of a cold cap are difficult to retrieve. Feeds treated in vertical temperature gradients reveal various features of cold caps (Choi et al., 2010), such as foam formation, but do not simulate the steady-state condition that characterizes the cold-cap melting process. Fortunately, it became possible to create cold caps in a laboratory-scale melter large enough to avoid bridging and small enough to allow quenching and preserving the cold-cap structure for detailed study (Kim et al., 2012; Dixon et al., 2013). Fig. 1 shows the fracture surface of a cold cap, confirming the reality of features originally identified based on crucible experiments and model calculations (see the left image in Fig. 1).

Confirming the cold-cap structure is just the first step. Continuing analysis will allow us to verify the distribution of individual phases, such as molten salts, crystalline phases, the glass-forming phase, and the gas phase, as well as the cold-cap properties, such as density. Feed samples heat-treated to various temperatures are being compared to sections through quenched cold caps using optical electron microscopy (Fig. 5).



Fig. 5. Scanning electron micrograph of feed heated to 900°C in a crucible (a) and a similarly structured region of the cold cap by optical (b) and electron (c) microscopy.

#### 4. Conclusions

A mathematical model has been developed to simulate the conversion of melter feed to molten glass that occurs within the cold cap. The model is capable of relating the performance and structure of the cold cap to the input variables that will eventually become available in the overall models of the melter. The model was applied to a melter feed formulated for a high-alumina, high-level waste for which the key properties needed for the model have been experimentally determined as functions of temperature and the heating rate. These properties are the bulk density, heat conductivity, effective heat capacity, melt foaminess, and kinetic equations for various feed reactions. The primary model output includes the rate of melting, cold-cap thickness, and secondary foam layer thickness. The model also yields the distribution of temperature, bulk and gas phase velocities, local heating rate, and concentration and crystal size of solid (quartz, hematite, or spinel) within the cold cap. Cold caps were produced in a laboratory-scale melter and preserved by quenching for detailed structural investigation to verify model assumptions and model results.

#### Acknowledgements

This project has been supported by the U.S. Department of Energy's Waste Treatment and Immobilization Plant Federal Project Office under the direction of Dr. Albert A. Kruger. The figures in this contribution were provided by Richard Pokorný, Derek Dixon, Jose Marcial, Jaehun Chun, and Brian Riley. Apart from the researchers just named, results presented are based on work of Carmen Rodrigues, David Pierce, Jarret Rice, Jarrod Crum, and Mike Schweiger. Discussions with Dong Kim and Albert Kruger continue and are greatly valued.

#### References

- Choi, A. S., Miller, D. H., Immel, D. M., 2010. Determination of HLW Glass Melt Rate Using X-Ray Computed Tomography, SRNL-STI-2010-00767, Savannah River National Laboratory, Aiken, South Carolina.
- Chun, J., Pierce, D. A., Pokorný, R., Hrma, P., 2013. Cold-Cap Reactions in Vitrification of Nuclear Waste Glass: Experiments and Modeling. *Thermochimica Acta* 559, 32–39.
- Dixon, D. R., Schweiger, M. J., Hrma, P., 2013. Effect of Feeding Rate on the Cold Cap Configuration in a Laboratory-Scale Melter. WM2013 Conference, February 24–28, Phoenix, Arizona, USA.
- Dolan, M. D., Misture, S. T., 2004. Analysis of Glass Batch Reactions Using *In Situ* X-Ray Diffraction. *Glass Technology* 45, 140–147, 167–174, 212–219.
- Henager, S. H., Hrma, P., Swearingen, K. J., Schweiger, M. J., Marcial J., TeGrotenhuis, N. E., 2011. Conversion of Batch to Molten Glass, I: Volume Expansion. *Journal of Non-Crystalline Solids* 357, 829–835.
- Hrma P., 1990. Melting of Foaming Batches: Nuclear Waste Glass. *Glastechnische Berichte* 63K, 360–369.
- Hrma, P., 1982. Thermodynamics of Batch Melting. *Glastechnische Berichte* 55, 138–150.
- Hrma, P., Kruger, A. A., Pokorný, R., 2012. Nuclear Waste Vitrification Efficiency: Cold Cap Reactions. *Journal of Non-Crystalline Solids* 358, 3559–3562.

- Hрма, P., Marcial, J., 2011. Dissolution Retardation of Solid Silica During Glass-Batch Melting. *Journal of Non-Crystalline Solids* 357, 2954–2959.
- Hрма, P., Schweiger, M. J., Humrickhouse, C. J., Moody, J. A., Tate, R. M., Rainsdon, T. T., TeGrotenhuis, N. E., Arrigoni, B. M., Marcial, J., Rodriguez, C. P., Tincher, B. H., 2010. Effect of Glass-Batch Makeup on the Melting Process. *Ceramics-Silikaty* 54, 193–211.
- Hрма, P., Swearingen, K. J., Henager, S. H., Schweiger, M. J., Marcial, J., TeGrotenhuis, N. E., 2011. Conversion of batch to molten glass, II: Dissolution of quartz particles. *Journal of Non-Crystalline Solids* 357, 820–828.
- Hрма, P., Vienna, J. D., 2000. Balancing Cost and Risk by Optimizing the High-Level Waste and Low-Activity Waste Vitrification. *Waste Management '00*, University of Arizona, Tucson, Arizona, USA.
- Kim, D. S., Schweiger, M. J., Buchmiller, W. C., Matyas, J., 2012. Laboratory-Scale Melter for Determination of Melting Rate of Waste Glass Feeds. PNNL-21005; EMSP-RPT-012, Pacific Northwest National Laboratory, Richland, Washington.
- Matlack, K. S., Kot, W. K., Callow, R. A., Innocent, J., Pegg, I. L., 2013. Testing of Optimized Bubbler Configuration for HLW Melter. VSL-13R2950-1, Vitreous State Laboratory, The Catholic University of America, Washington, D.C.
- Matyas, J., Vienna, J. D., Kimura, A., Schaible, M. J., Tate, R. M., 2010. *Ceramic Transactions* 222, 41–51.
- Mika, M., Hрма, P., Schweiger, M. J., 2000. Rheology of Spinel Sludge in Molten Glass. *Ceramics-Silikaty* 44, 86–90.
- Pierce, D. A., Hрма, P., Marcial, J., 2012a. Thermal Analysis of Waste Glass Batches: Effect of Batch Makeup on Gas-Evolving Reactions, Chapter 20. In: Šesták, J., Šimon, P., (Ed.). *Thermal Analysis of Micro, Nano- and Non-Crystalline Materials*. Springer, Dordrecht, pp. 429–40.
- Pierce, D. A., Hрма, P., Marcial, J., Riley, B. J., Schweiger, M. J., 2012b. Effect of Alumina Source on the Rate of Melting Demonstrated with Nuclear Waste Glass Batch. *International Journal of Applied Glass Science* 3, 59–68.
- Pokorny, R., Hрма, P., 2012. Mathematical Modeling of Cold Cap. *Journal of Nuclear Materials* 429, 245–56.
- Pokorny, R., Hрма, P., 2014. Model for the conversion of nuclear waste melter feed to glass. *Journal of Nuclear Materials* 445, 190–199.
- Pokorny, R., Pierce, D. A., Hрма, P., 2012. Kinetics of Batch-Melting Reactions. *Thermochimica Acta* 541, 8–14.
- Pokorny, R., Rice, J. A., Crum, J. V., Schweiger, M. J., Hрма, P., 2013a. Kinetic Model for Quartz and Spinel Dissolution During Melting of High-Level-Waste Glass Batch. *Journal of Nuclear Materials* 443, 230–235.
- Pokorny, R., Rice, J. A., Schweiger, M. J., Hрма, P., 2013b. Determination of Temperature-Dependent Heat Conductivity and Thermal Diffusivity of Waste Glass Melter Feed, *Journal of the American Ceramic Society* 96, 1891–1898.
- Schill, P., 1982. Mathematical Model of Batch Melting in All-Electric Furnaces. *Ceramics-Silikaty* 26, 155–163, 209–222.
- Schill, P., Lutze, W., Gong, W., Pegg, I. L., 2007. Testing and Modeling the Behaviour of Platinoids During Vitrification of High Level Radioactive Waste, Part 2. *Glass Technology-Part A* 48, 276–289.
- Schweiger, M. J., Hрма, P., Humrickhouse, C. J., Marcial, J., Riley, B. J., TeGrotenhuis, N. E., 2010. Cluster Formation of Silica Particles in Glass Batches During Melting. *Journal of Non-Crystalline Solids* 356, 1359–1367.